Intermetallics 20 (2012) 176–182

Contents lists available at SciVerse ScienceDirect

Intermetallics

journal homepage: www.elsevier.com/locate/intermet

Short communication

On the new ternary $RZnSn_2$ compounds with $HfCuSi_2$ structure type

Yu. Verbovytskyy[a,*], K. Łątka[b], J. Przewoźnik[c], N. Leal[d], A.P. Gonçalves[a]

[a] Departamento de Química, Instituto Tecnológico e Nuclear/CFMC-UL, Estrada Nacional 10, P-2686-953 Sacavém Codex, Portugal
[b] M. Smoluchowski Institute of Physics, Jagiellonian University, Reymonta 4, 30-059 Kraków, Poland
[c] AGH University of Science and Technology, Faculty of Physics and Applied Computer Science, Department of Solid State Physics, Ave. Mickiewicza 30, 30-059 Krakow, Poland
[d] Centro de Investigação em Ciência e Engenharia Geológica, Departamento de Ciências da Terra – Faculdade de Ciências e Tecnologia, Universidade Nova de Lisboa (CICEGe/DCT – FCT/UNL), Campus de Caparica, 2829-516 Caparica, Portugal

ARTICLE INFO

Article history:
Received 21 July 2011
Received in revised form
23 August 2011
Accepted 31 August 2011
Available online 29 September 2011

Keywords:
A. Rare-earth intermetallics
B. Crystal chemistry of intermetallics
B. Phase identification
F. Diffraction
B. Magnetic properties

ABSTRACT

Seven new ternary $RZnSn_2$ (R = Y, Gd, Dy, Ho, Er, Tm, Lu) compounds have been synthesized by reacting the elements at ~1000 °C, followed by annealing at 400 °C. The crystal structure of the all compounds was solved from powder X-ray counter data and their compositions were confirmed by EDS analysis. It was found that the new compounds crystallize with tetragonal $HfCuSi_2$ structure type. Ferromagnetic-like magnetisation curves are observed for $YZnSn_2$ and $LuZnSn_2$ with puzzling magnetisation $\sigma(H)$ oscillations for the last one, while for $RZnSn_2$ with Ho, Er and Tm antiferromagnetic ordering takes place at low temperatures.

1. Introduction

A large number of intermetallic compounds with general composition $RM_{1\pm x}T_{2\pm y}$ or idealized RMT_2 (R – rare earth, M – *d*-metal and T – *p*-metal) have been found in many ternary R–M–T systems [1]. Among them, zinc-based compounds with antimony and bismuth were found with the tetragonal $HfCuSi_2$ structure type, having significant defected position of zinc atoms: $RZn_{\sim 0.6}Sb_2$ (R = La, Ce, Pr, Nd, Sm, Gd, and Tb) [2–6] and $RZn_{\sim 0.5}Bi_2$ (R = La, Ce, and Pr) [4,7], respectively. Evidence of polymorphic transformation from tetragonal $HfCuSi_2$-type to orthorhombic $NdAgSb_2$-type at high temperature (~600–800 °C) has been detected for the ternary $LaZn_{0.6}Sb_2$ and $CeZn_{0.8}Sb_2$ antimonides [5]. Early reported [8] ternary praseodymium zinc arsenide $Pr_3Zn_2As_6$ (=$PrZn_{2/3}As_2$) was to be described as an ordered defected version of the $HfCuSi_2$ structure type. Authors of [9] determined the crystal structure of ternary $TbZnSn_2$ compound with fixed 1:1:2 composition based on single crystal data.

The present work is the continuation of our previous investigations (phase diagrams analysis, crystal structures determination and properties of intermetallic compounds) on the interaction among the components containing rare earth, zinc and *p*-metals [10–16]. Herein we present the crystal structure and magnetic investigations carried out on the new ternary $RZnSn_2$ stannides.

2. Experimental details

Metals with nominal purities 99.9 wt.% (rare earth ingots) and 99.97 wt.% (zinc tear drops and gallium pieces) were used as starting materials. The ternary R–Zn–Sn (R = Y, Gd, Tb, Dy, Ho, Er, Tm, Lu) alloys with nominal composition $R_{25}Zn_{25}Sn_{50}$ have been prepared in evacuated quartz tubes at 1000 °C and further annealed at 400 °C during one month. The obtained samples were studied by X-ray powder diffraction and EDS analyses. Due to the instability (oxidation) under normal conditions, all alloys were stored at low temperature (−18 °C).

X-ray phase and structural studies were performed using a PANalytical X'Pert Pro diffractometer (Cu Kα-radiation). The scans were taken in the $\theta/2\theta$ mode with the following parameters: 2θ region, 15–100°; step scan, 0.03°; counting time per step, 30 s. The lattice parameters were obtained by least-squares fitting using the Latcon program [17]. The FullProf [18] program was used for Rietveld refinements.

A JEOL Scanning Microscope JSM-T330A, coupled with an energy dispersive X-ray spectroscopy (EDS) device, was used both to observe the morphology on polished surfaces of selected samples, and to obtain chemical data for the composition of the

* Corresponding author.
E-mail address: yuryvv@bigmir.net (Yu. Verbovytskyy).

0966-9795/$ – see front matter © 2011 Elsevier Ltd. All rights reserved.
doi:10.1016/j.intermet.2011.08.024

synthesized compounds. Acquisition parameters were: 25 kV accelerating voltage, 4–6 μA beam current, 200 s preset time for acquiring a spectrum, 2048 channels, 10 eV/Channel, 20 keV width, Si crystal detector, Al-coated protective window. For image capture, AnalySIS® 3.0 software, from Soft Imaging System GmbH, was used. The semi-quantitative chemical analyses were performed using Quest SpectraPlus software, from Thermo Noran.

Systematic magnetic susceptibility measurements were carried out in the DC mode at the fields 50 Oe, 1 kOe or at higher fields in the case of Y and Lu compounds (20 kOe, 40 kOe or 80 kOe) as well as hysteresis loops up to 90 kOe were made in the temperature range 1.9 K up to 200 K (depending on the sample) using the vibrating sample magnetometer (VSM) option of the Quantum Design physical property measurement system (PPMS). Especially, the measurements with VSM option at low external field $H_0 = 50$ Oe were applied since they enable investigations not significantly affecting the given magnetic system, and therefore they are well suited for a precise determination of magnetic phase transitions. The right zeroing of the magnetic field was made using the ultra-low field VSM option. In the zero field cooling mode (ZFC) the samples were first cooled down in absence of external magnetic field and then investigated while heating in a given magnetic field. On the other hand, the field cooling mode (FC) followed ZFC one in the same magnetic field and measurements were performed with decreasing temperature. For both modes, the cooling process always started from the paramagnetic state. The magnetic transition temperature was derived using numerical analysis of the obtained ZFC mass magnetisation curve $\sigma(T)$. During magnetic measurements step scanning was applied both for temperature as well as for the field variations.

3. Results and discussion

3.1. Crystal properties

Seven new ternary $RZnSn_2$ (R = Y, Gd, Dy, Ho, Er, Tm, Lu) phases were detected and one (R = Tb) phase was confirmed. The R/Zn/Sn = 1:1:2 compositions of the above mentioned compounds were confirmed by EDS analysis (within an experimental error of ~5%) and their crystal structures were solved from powder X-ray counter data, except for Tb and Dy samples, where significant amounts of unknown phases where observed. Due to the microcrystalline nature of the annealed $R_{25}Zn_{25}Sn_{50}$ alloys, the Rietveld method was applied for crystal structure refinement. Several structural (defected, ordered and disordered) models were tested. Reasonable results were obtained in case of an ordered model; the same was reported early for the $TbZnSn_2$ phase [8]. For example, the results of such refinement for the $Tm_{25}Zn_{25}Sn_{50}$ alloys are shown in Fig. 1. Crystallographic data, atom parameters and thermal displacement parameters are presented in Tables 1 and 2. The unit cell volume as a function of the atomic number is shown in Fig. 2, which is gradually decrease along the R (Gd → Lu) series indicating the so-called lanthanide contraction mechanism.

The $RZnSn_2$ compounds belong to the tetragonal $HfCuSi_2$ structure type (*P*4/*nmm* space group) (Fig. 3). Rare earth metals occupy the Hf position and they are located inside deformed cuboctahedra (coordination number 12). Zinc atoms situated in Cu site; coordination polyhedra for these atoms are also deformed cuboctahedra (CN = 12). Big tin atoms are positioned in the Si site. Intergrowth double trigonal prisms (CN = 8) and tetragonal antiprisms (CN = 8) are the polyhedra for the tin atoms.

The shortest interatomic distances for the ternary $RZnSn_2$ compounds are shown in Table 3. Significantly shorter contacts could be observed for the R–Sn, Zn–Sn and Sn–Sn atoms. However,

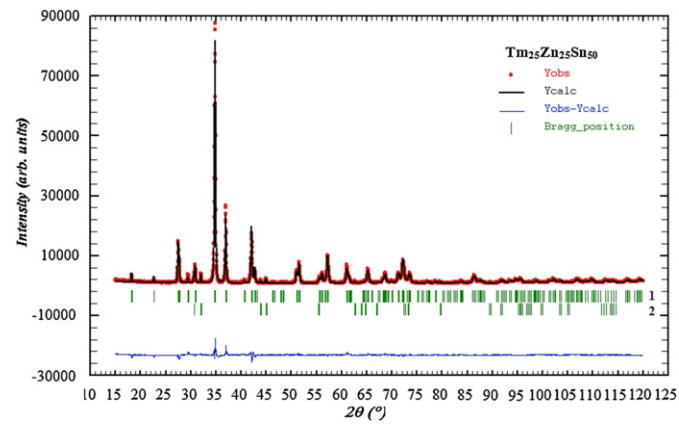

Fig. 1. X-ray diffraction pattern of the annealed $Tm_{25}Zn_{25}Sn_{50}$ alloy (1 – $TmZnSn_2$, 2 – Sn).

the R–Zn and Zn–Zn distances are large than the sum of the atomic radii of the respective atoms [19].

Comparing the structure of $RZnT_2$ (1:1:2) ($HfCuSi_2$-type) compounds with other known ones from rare earth – zinc – *p*-metal system, it should be noticed the frequent existence of the $RZn_{2-x}T_{2+x}$ ($0 \le x \le 1$) compounds with $BaAl_4$-type (or its derivatives), which is related to $HfCuSi_2$-type. Among $RZn_{2-x}T_{2+x}$ compounds, the ternary $EuZn_2Sn_2$ (two modifications with $CaBe_2Ge_2$ and $LaPt_2Ge_2$ types), RZn_2T_2 (R = Eu, Yb; T = Si, Ge; $CeAl_2Ga_2$-type) $RZn_{2-x}T_{2+x}$ (R = La–Dy; T = Al, Ga; $CeAl_2Ga_2$ or $BaAl_4$-type) compounds are known from the literature [11–13,16,20–23]. For example, Fig. 4 illustrated the relationship between structures of the $RZnSn_2$ ($HfCuSi_2$-type) and RZn_2Al_2 ($CeAl_2Ga_2$-type, superstructure of $BaAl_4$-type) compounds. The $BaAl_4$ structure type described here as a filled version of the $HfCuSi_2$-type. The $RZnSn_2$ structure can be presented like alternation of two 2D layers (condensed $ZnSn_4$ tetrahedra and square Sn nets) along *c* axes separated by rare earth atoms (Fig. 4a). In case of RZn_2Al_2, small Zn and Al atoms form three-dimensional network with rare earth atoms inside (Fig. 4b).

3.2. Magnetic properties

The results of the bulk magnetic measurements obtained for $RZnSn_2$ (R = Y, Ho, Er, Tm, Lu) are shown in Figs. 5–9 and the basic magnetic parameters derived for antiferromagnetic compounds with Ho, Er and Tm are collected in Table 4.

The magnetic measurements of YZn_2Sn_2 and $LuZn_2Sn_2$ revealed that they are not magnetically ordered down to 1.9 K, as their susceptibilities, $\chi_\sigma(T)$, do not show any magnetic anomaly and have small values (of an order 10^{-7}–10^{-8} cm^3/g, Fig. 5). The non-

Table 1
Calculated lattice parameters for the $RZnSn_2$ intermetallic compounds ($HfCuSi_2$-type, *P*4/*nmm* space group, *Z* = 2).

R	Lattice parameters		
	a (Å)	*c* (Å)	*V* (Å^3)
Y	4.3234(1)	9.8612(4)	184.32(1)
Gd	4.3506(1)	9.9374(3)	188.10(1)
Tb	4.3306(3)	9.8568(6)	184.85(2)
Dy	4.3158(3)	9.8136(5)	182.79(2)
Ho	4.3087(1)	9.7816(3)	181.60(1)
Er	4.2990(1)	9.7560(2)	180.30(1)
Tm	4.2913(1)	9.7281(3)	179.15(1)
Lu	4.2835(1)	9.6903(3)	177.80(1)

Table 2
Atomic and thermal parameters in the structure of the $RZnSn_2$ intermetallic compounds.

R	Y	Gd	Ho	Er	Tm	Lu
Atomic and thermal parameters						
R (¼ ¼ *z*),	0.24960(28)	0.25160(24)	0.25001(21)	0.24925(16)	0.24930(14)	0.24898(20)
B_{iso} (Å^2)	0.52(7)	0.48(7)	1.23(6)	0.77(4)	0.84(4)	0.99(5)
Zn (¾ ¼ ½),						
B_{iso} (Å^2)	0.86(11)	0.99(15)	0.60(5)	1.28(8)	1.20(8)	1.06(13)
Sn1 (¾ ¼ 0),						
B_{iso} (Å^2)	0.65(7)	1.45(7)	0.73(5)	0.65(5)	0.68(5)	0.75(7)
Sn2 (¼ ¼ *z*),	0.68413(20)	0.68477(27)	0.68878(18)	0.68705(17)	0.68899(15)	0.68972(24)
B_{iso} (Å^2)	1.73(6)	1.45(7)	0.73(5)	1.46(4)	1.49(4)	1.31(6)
Reliability factors						
R_B (%)	5.37	9.75	8.65	6.09	5.16	5.44
R_p (%)	8.25	9.55	8.22	6.75	5.39	3.87

Curie–Weiss nature of the two obtained curves suggests the absence of a localized magnetic moment in both compounds under discussion.

The magnetisation isotherms, $\sigma(H)$, for the YZn_2Sn_2 and $LuZn_2Sn_2$ samples are shown in Fig. 6. Surprisingly, for these samples the magnetic states are very sensitive to applied magnetic external fields leading to non-linear dependencies of the recorded magnetisation curves at the lowest temperatures. Generally, such a non-linear behaviour can be attributed to paramagnetic or ferromagnetic impurities or to a field-induced ferromagnetism. Since the observed effect for the resulting magnetisations at 9 T is very weak (of an order of 10^{-3} μ_B/f.u.), the possible level of ferromagnetic impurities is small, corresponding to 500 ppm. One can note, however, that routinely made zero and low field magnetisation scans versus temperature ($M(T)$) for Y and Lu samples do not confirm any magnetic transition detectable for them. Assuming the absence of localized magnetic moments, a non-linear increase of recorded magnetisations can be associated with induced magnetic moments of conduction electrons. For YZn_2Sn_2 at 1.9 K and 4.2 K hysteretic behaviours can be registered, while at elevated temperatures the non-linear $\sigma(H)$ dependence still survives. The most striking findings are the relatively regular magnetisation oscillations observed for the Lu compound at high fields and up to 20 K. It was checked experimentally that these oscillations are reproducible and are not influenced by the value of the applied VSM vibration amplitude (as can be seen in Fig. 6, the $\sigma(H)$ dependence recorded at 4.2 K is practically the same for the routinely used 2 mm amplitude as well as for the 1 mm one). In this context, it is worth to note that the observed oscillations decrease with the increasing temperature, the recorded $\sigma(H)$ variation at $T = 50$ K being already linear. This fact needs, certainly, a further elucidation. However, it is well known (see for example [24] and [25]) that oscillatory effects in metals caused by external fields at low temperatures are a characteristic phenomena revealed by resistivity, magnetic susceptibility (magnetisation) or heat capacity oscillations observed in strong enough magnetic fields. Therefore, and albeit the polycrystalline nature of the samples, it is really tempting to prescribe the revealed effect to such phenomenon. Nevertheless, to support this idea new experiments made on a monocrystals are in fact urgently needed.

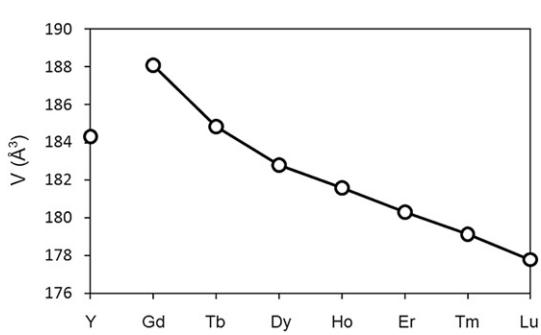

Fig. 2. Unit cell volume versus atomic number.

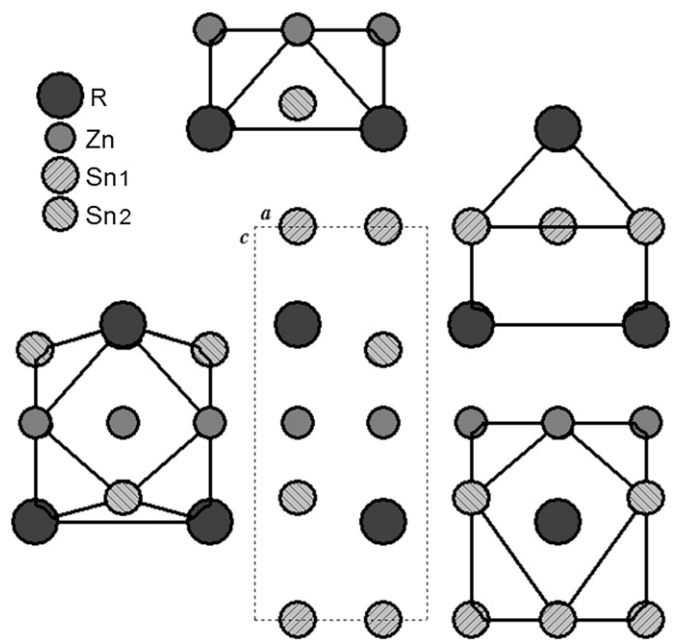

Fig. 3. Projection of the crystal structure of the $RZnSn_2$ compounds on the *xy* plane and coordination atoms polyhedra. Black circles indicated rare earth (R) atoms, grey filled circles are Zn atoms, and Sn atoms are marked by light hatching circles.

The temperature dependencies of the magnetic mass susceptibility $\chi_\sigma(T)$ observed for the compounds with Ho, Er and Tm and their inverses $1/\chi_\sigma(T)$ measured in a field of $H_0 = 1000$ Oe are presented in Fig. 7. At high temperatures, $\chi_\sigma(T)$ data were successfully adjusted by a modified Curie–Weiss law in the form $\chi_\sigma = \chi_0 + C/(T - \theta_p)$. The obtained temperature independent

Table 3
Selected interatomic distances (Å) for the $RZnSn_2$ intermetallic compounds.

R	Y	Gd	Ho	Er	Tm	Lu
R–Sn1	3.276(2)	3.314(2)	3.259(2)	3.246(1)	3.238(1)	3.226(1)
R–Sn2	3.126(1)	3.141(1)	3.105(1)	3.103(1)	3.093(1)	3.087(1)
R–Zn	3.282(2)	3.290(2)	3.259(2)	3.257(1)	3.248(1)	3.241(1)
Zn–Zn	3.057(1)	3.076(1)	3.047(1)	3.040(1)	3.034(1)	3.029(1)
Zn–Sn2	2.823(1)	2.847(2)	2.837(1)	2.820(1)	2.826(1)	2.823(2)
Sn1–Sn1	3.057(1)	3.076(1)	3.047(1)	3.040(1)	3.034(1)	3.029(1)

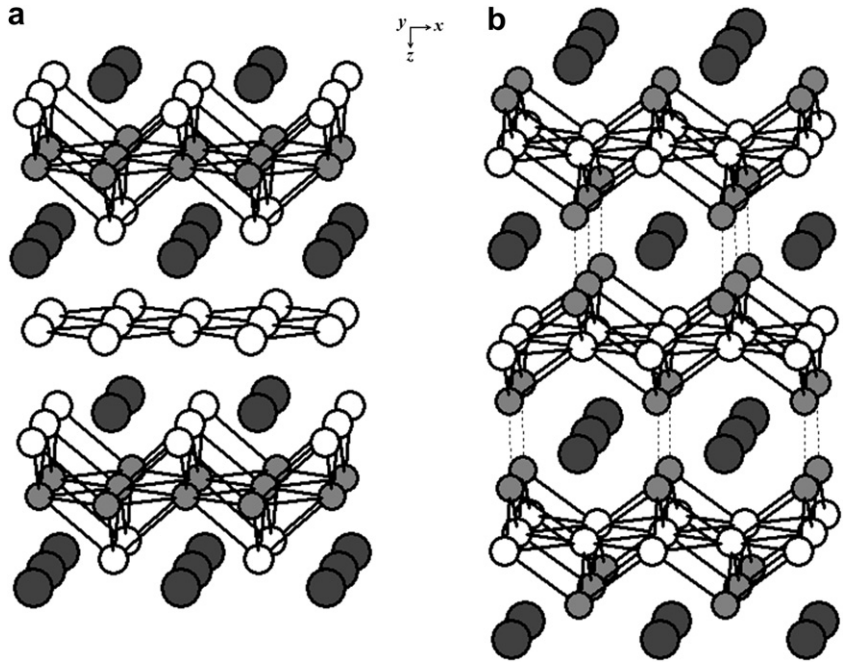

Fig. 4. Relationship between $RZnSn_2$ ($HfCuSi_2$-type) (a) and RZn_2Al_2 ($CeAl_2Ga_2$-type) (b). Rare earth, zinc and T (Sn and Al) atoms are shown by dark, grey and white circles, respectively.

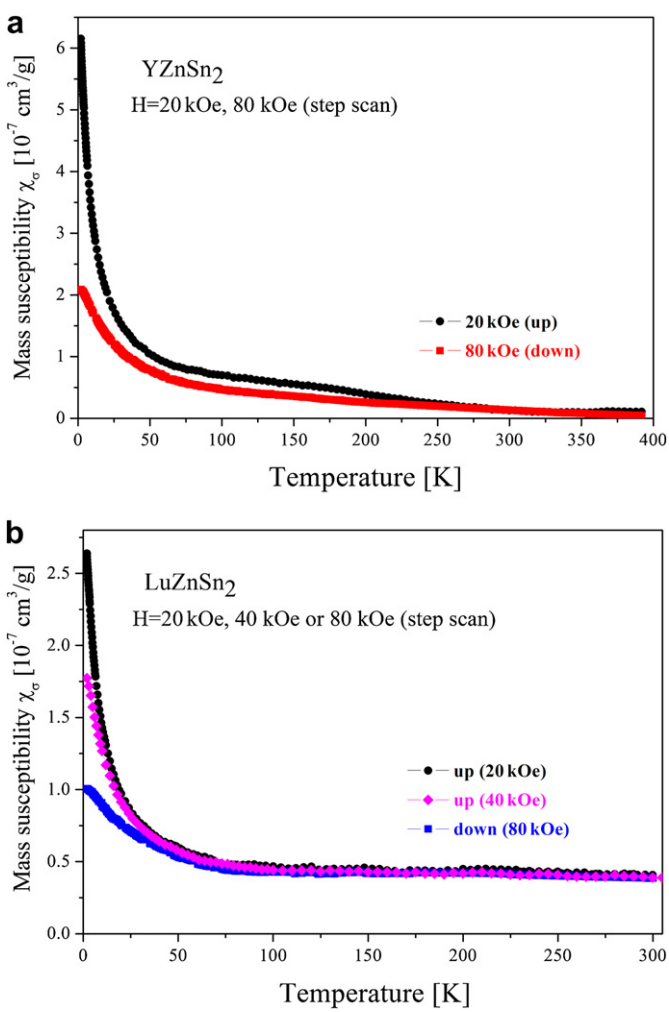

Fig. 5. Temperature dependencies of the magnetic susceptibilities for $YZnSn_2$ (a) and $LuZnSn_2$ (b) as measured with a PPMS using VSM in different external magnetic fields *H*.

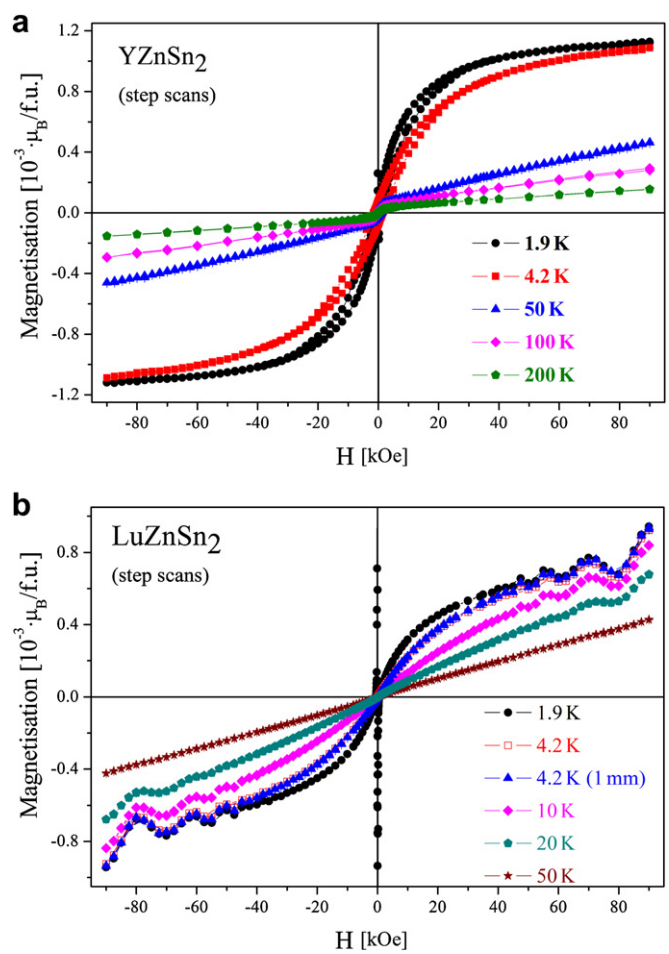

Fig. 6. Field dependence of the magnetisation at different temperatures for: $YZnSn_2$ (a) and $LuZnSn_2$ (b) as measured with a PPMS VSM option (note that two independent measurements were made at 4.2 K, i.e. one with routinely used 2 mm VSM vibration amplitude and the second one with 1 mm amplitude, with no evident influence on the $\sigma(H)$ dependence).

factors, χ_0, the Curie constants, C, and the paramagnetic Curie temperatures, θ_p, are summarized in the Table 4. The clearly negative values of θ_p are indicative for antiferromagnetic interactions. The effective magnetic moments were derived from the formula $\mu_{eff} = p_{eff} \times \mu_B$, where $p_{eff} = (3k_B/N_A)^{1/2} \times (MC)^{1/2}/\mu_B$ (here k_B is the Boltzmann constant, N_A is the Avogadro number and M is the molar mass expressed in grams). It is worth to note that the obtained experimental values μ_{eff} are systematically higher than the theoretical 3+ free-ion values $\mu_{eff} = g\mu_B[J(J+1)]^{1/2}$ for all these three compounds. Such a behaviour might be explained in terms of strong coupling (polarization) of the conduction electrons with the

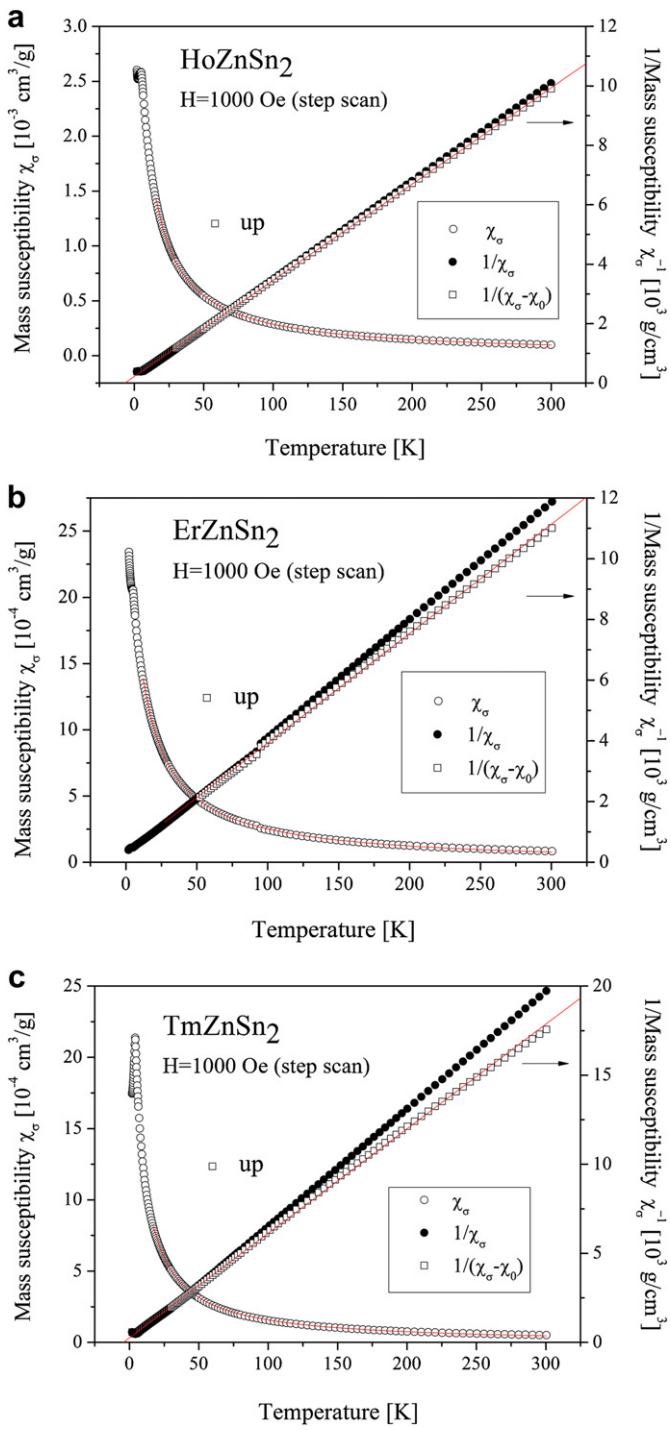

Fig. 7. Temperature dependence of the magnetic susceptibilities (left-hand scale) and inverse susceptibilities (right-hand scale) for $HoZnSn_2$ (a), $ErZnSn_2$ (b) and $TmZnSn_2$ (c) as measured with a PPMS using VSM in an external magnetic field $H = 1000$ Oe. In the inset, the magnetic parameters obtained from the fit represented by continuous line according to a modified Curie–Weiss law are presented, as explained in the text. The observed magnetic anomalies point to the paramagnetic – antiferromagnetic transitions (see Table 4) agreeing well with those obtained from the low field magnetic measurements in an external magnetic field $H = 50$ Oe (see Fig. 8).

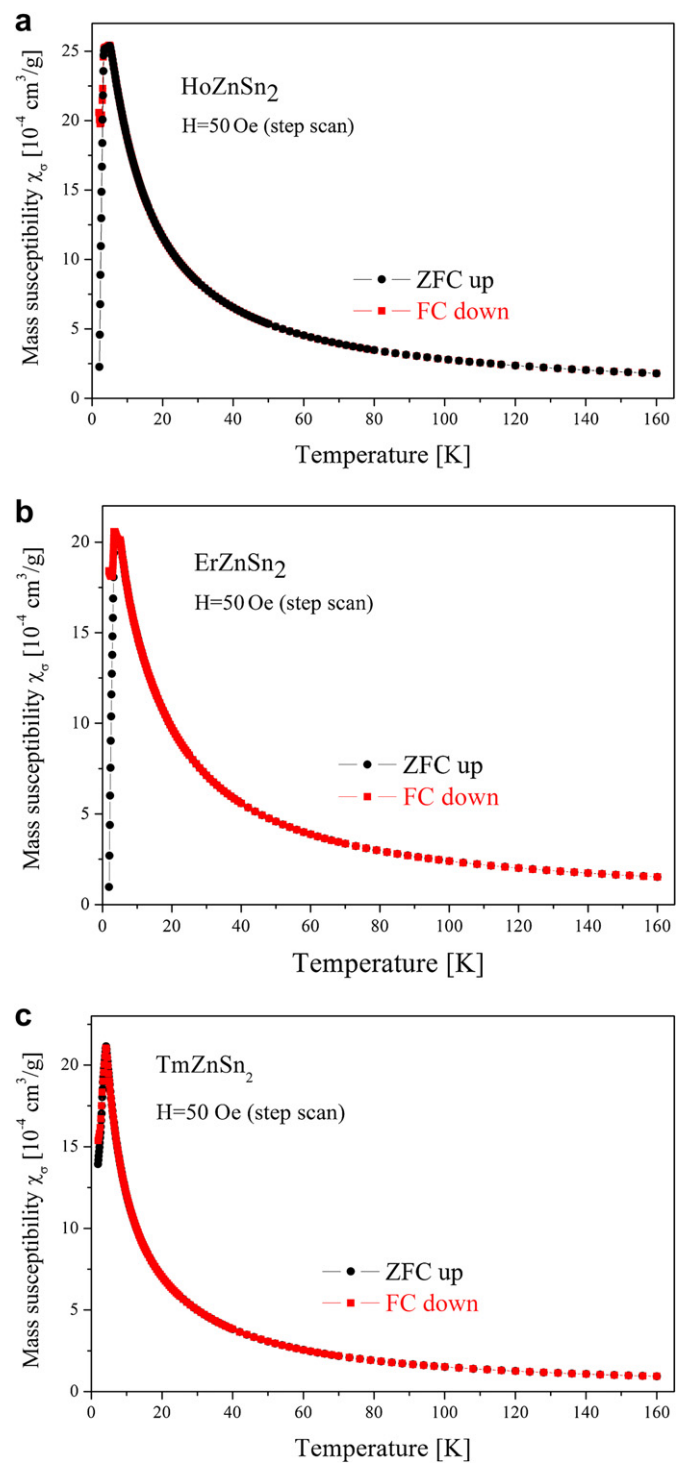

Fig. 8. Temperature dependence of the magnetic susceptibilities for $HoZnSn_2$ (a), $ErZnSn_2$ (b) and $TmZnSn_2$ (c) as measured with a PPMS using low field VSM option in an external magnetic field $H = 50$ Oe. ZFC curve was recorded with rising temperature while FC one with decreasing temperature.

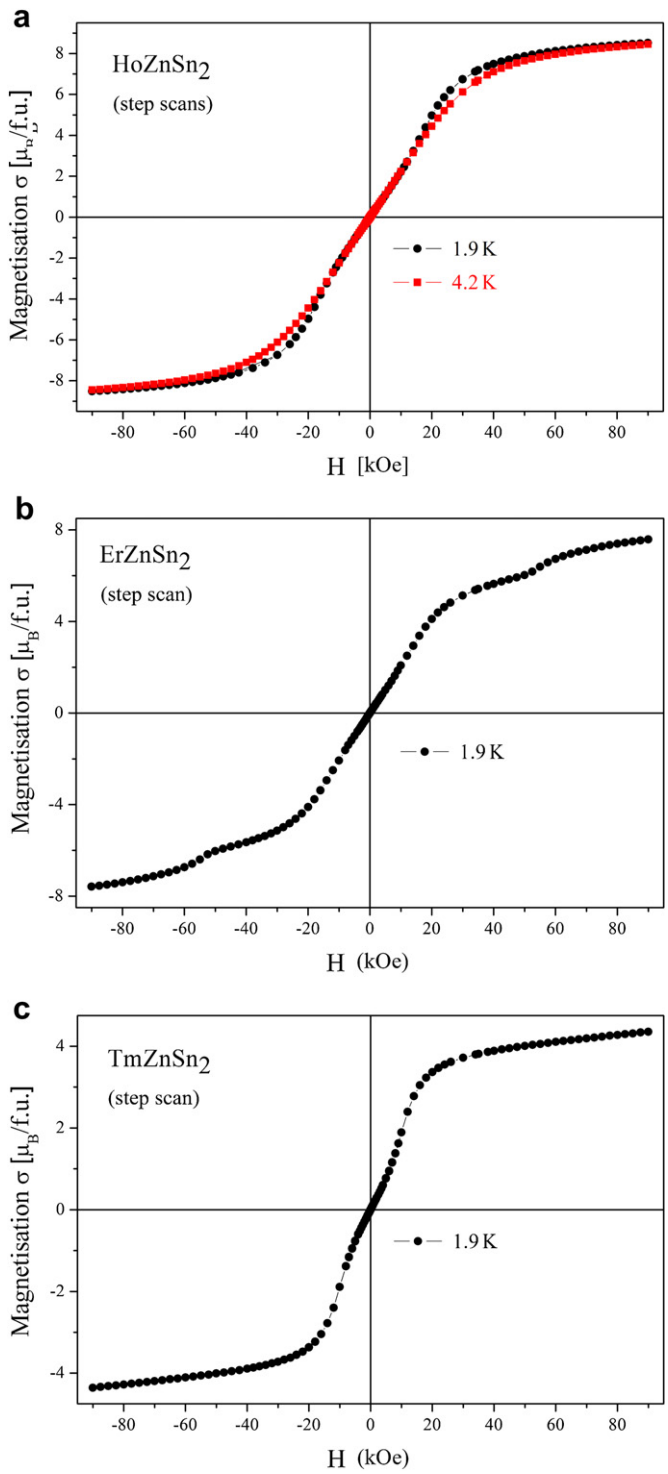

Fig. 9. Field dependence of the magnetisations σ isotherms for $HoZnSn_2$ (a), $ErZnSn_2$ (b) and $TmZnSn_2$ (c) as measured with a PPMS VSM option at $T = 1.9$ and/or $T = 4.2$ K, respectively.

Table 4
Magnetic data for $RZnSn_2$ (R = Ho, Er and Tm) compounds.

Compound	χ_0 ($\times 10^{-6}$ cm^3/g)	θ_p (K)	μ_{eff} (μ_B)	$\mu_{eff}^{(theor.)}$ (μ_B)	T_N (K)	
$HoZnSn_2$	−1.995	−5.8	11.31	10.61	4.9(1)	AF
$ErZnSn_2$	−6.70	−8.8	10.47	9.58	5.0(1)	AF
$TmZnSn_2$	−6.30	−4.3	8.16	7.56	4.1(1)	AF

AF – antiferromagnetic ordering.

individual rare earth localized moments and the resulting excess moments can be tentatively prescribed to the contribution coming from d-electrons of Zn.

The antiferromagnetic character of the observed magnetic anomalies presented in Fig. 7 was fully confirmed by low field magnetic measurements at $H = 50$ Oe as displayed in Fig. 8 where ZFC and FC magnetic results for corresponding mass susceptibilities, $\chi_\sigma(T)$, are collected. It is seen that in each case ZFC and FC curves fits altogether almost exactly, except of the FC dependence observed for $ErZnSn_2$ at low temperatures (much below its antiferromagnetic maximum) where the abrupt fall of ZFC variation can be prescribed to a possible tiny amount (not detected by X-ray diffraction) of diamagnetic tin impurity. Numerical analysis of the first and the second derivatives obtained for the corresponding ZFC curves was used to determine the individual antiferromagnetic transition Néel temperatures, T_N, being equal to 4.9(1) K, 5.0(1) K and 4.1(1) K for $HoZnSn_2$, $ErZnSn_2$ and $TmZnSn_2$, respectively.

Magnetisation measurements versus magnetic fields, at 1.9 K and/or 4.2 K and in the −90 kOe to +90 kOe range, are displayed in Fig. 9. At 90 kOe and 1.9 K the magnetisation values, σ, are 8.52 μ_B, 7.58 μ_B and 4.35 μ_B per a given rare earth atom for $HoZnSn_2$, $ErZnSn_2$ and $TmZnSn_2$, respectively. These values are not far away from the expected theoretical saturation magnetic moments $\mu_s = gJ$, i.e. 10.0 μ_B/Ho, 9.0 μ_B/Er and 7.0 μ_B/Tm. However, it is clear that the maximal experimental magnetic field is not big enough to get saturation. A closer inspection of the obtained magnetisation curves shows that the Ho, Er and Tm compounds undergo metamagnetic transitions (corroborating their antiferromagnetic ordering) in fields H_{SF} (SF means spin flop), which can be roughly estimated as 12 kOe, 11 kOe and 10 kOe, respectively. Moreover, for $ErZnSn_2$ two additional transitions that can be associated with field-induced spin reorientations take place at about 30 kOe and 58 kOe.

4. Conclusions

The new ternary intermetallic compounds $RZnSn_2$ (R = Y, Gd, Tb, Dy, Ho, Er, Tm, Lu) were synthesized at ~1000 °C and their crystal structure was derived from X-ray diffraction data. These compounds crystallize in the tetragonal $HfCuSi_2$ structure type (*P*4/*nmm* space group).

Experimental results support the idea that for the Y and Lu compounds the magnetic behaviour is dominated by conduction electrons. They show ferromagnetic-like magnetisations $\sigma(H)$ at the lowest temperatures, with an astonishing oscillatory character revealed by $LuZnSn_2$ at high magnetic fields. $HoZnSn_2$, $ErZnSn_2$ and $TmZnSn_2$ undergo antiferromagnetic-like transitions at 4.9(1) K, 5.0(1) K and 4.1(1) K, respectively.

Acknowledgements

This work was partially supported by FCT, Portugal, under the contract No. PTDC/CTM/102766/2008. The FCT Grant No. SFRH/BPD/34840/2007 for the research work of Y.V. at ITN, Sacavém, Portugal is highly appreciated.

The magnetic measurements were carried out with the PPMS – Quantum Design equipment purchased thanks to the financial support of the European Regional Development Fund in the framework of the Polish Innovation Economy Operational Program (contract no. POIG.02.01.00–12–023/08).

Appendix. Supplementary data

Supplementary data related to this article can be found online at doi:10.1016/j.intermet.2011.08.024.

References

[1] Villars P, editor. Pearson's handbook, crystallographic data for intermetallic phases (desk ed.). OH: ASM Materials Park; 1997.
[2] Sologub O, Hiebl K, Rogl P, Bodak O. Ternary compounds $REMSb_2$ RE = La, Ce, Pr, Nd, Sm, Gd, Tb; M = Mn, Zn, Cd; compound formation, crystal structure and magnetism. J Alloys Compd 1995;227:40–3.
[3] Wollesen P, Jeitschko W, Brylak M, Dietrich L. Ternary antimonides $LnM_{1-x}Sb_2$ with Ln = La–Nd, Sm, Gd, Tb and M = Mn, Co, Au, Zn, Cd. J Alloys Compd 1996;245:l5–8.
[4] Flandorfer H, Sologub O, Godart C, Hiebl K, Leithe-Jasper A, Rogl P, et al. On the cerium valence in ternary compounds $CeMSb_2$ and $CeM'Bi_2$; M = Mn, Fe, Co, Ni, Cu, Zn, Pd, Ag, Au and M′ = Ni, Cu, Zn, Ag. Solid State Commun 1999;97: 561–5.
[5] Salamakha LP, Mudryi SI. Crystal structure of the $RZn_{1-x}Sb_2$ compounds (R = La, Ce). J Alloys Compd 2003;359:139–42.
[6] Zelinska OYa, Mar A. Structure and physical properties of rare-earth zinc antimonides $REZn_{1-x}Sb_2$ (RE = La, Ce, Pr, Nd, Sm, Gd, Tb). J Solid State Chem 2006;179:3776–83.
[7] Zelinska OYa, Mar A. Structure and electrical resistivity of rare–earth zinc bismuthides $REZn_{1-x}Bi_2$ (RE = La, Ce, Pr). J Alloys Compd 2008;451:606–9.
[8] Nientiedt AT, Jeitschko W. The praseodymium zinc arsenide $Pr_3Zn_2As_6$: crystallizing with a vacancy variant of the HfCuSi2 type structure. J Solid State Chem 1999;142:266–72.
[9] Pavlyuk V, Oshchapovsky I, Marciniak B. Crystal structure of the $TbZnSn_2$ and TbZnSn ternary compounds. J Alloys Compd 2009;477:145–8.
[10] Verbovytskyy Yu, Gonçalves AP. The Yb–Zn–In system at 400 °C: partial isothermal section with 0–33.3 at.% Yb. J Alloys Compd 2009;486: 148–53.
[11] Verbovytskyy Yu, Gonçalves AP. The Yb–Zn–Ga system: partial isothermal section at 400 °C with 0–33.3 at.% Yb. Intermetallics 2010;18:655–65.
[12] Verbovytskyy Yu, Alves LC, Gonçalves AP. Phase relations of the Eu–Zn–Al system at 400 °C from 0 to 33.3 at.% Eu. J Alloys Compd 2010;495:39–44.
[13] Verbovytskyy Yu, Kaczorowski D, Gonçalves AP. Novel RZn_2Ga_2 (R = La, Ce, Pr, Nd, Sm) intermetallic compounds with $BaAl_4$-type structure. J Alloys Compd 2010;508:20–3.
[14] Verbovytskyy Yu, Pereira LCJ, Gonçalves AP. Crystal structure and magnetic properties of $YbZn_{8.3-9.2}Ga_{2.7-1.8}$ with $BaHg_{11}$. J Alloys Compd 2011;509: L14–7.
[15] Verbovytskyy Yu, Kaczorowski D, Gonçalves AP. On new ternary phases from Eu–Zn–T (T = Al and Ga) systems. Intermetallics 2011;19:613–20.
[16] Verbovytskyy Yu, Leal N, Gonçalves AP. New representatives with $BaAl_4$, La_3Al_{11} and $BaHg_{11}$ structure types from the R–Zn–Ga ternary systems (R = Y, Lu, Gd–Tm). Intermetallics 2011;19:1080–4.
[17] Schwarzenbach D. Program LATCON. Switzerland: University of Lausanne; 1975.
[18] Rodriguez-Carvajal J, Roisnel T. FullProf.98 and WinPLOTR: New Windows 95/NT applications for diffraction commission for powder diffraction. International Union for Crystallography, Newsletter (May–August) Summer, 1998; 20.
[19] Bokiy GB. Crystal chemistry. 3rd ed. Moscow: Nauka; 1971 [in Russian].
[20] Stel'makhovych B, Stel'makhovych O, Kuz'ma Yu. New intermetallic compounds in the RE–Zn–Al systems and their crystal structure. J Alloys Compd 2005;397:115–9.
[21] Dhar SK, Paulose P, Kulkarni R, Manfrinetti P, Pani M, Parodi N. Crystal structure and magnetic ordering in dimorphic $EuZn_2Sn_2$. Solid State Commun 2009;149:68–72.
[22] Grytsiv A, Leithe-Jasper A, Flandorfer H, Rogl P, Hiebl K, Godart C, et al. Novel ytterbium-zinc-silicides and germanides grown from zinc-flux. J Alloys Compd 1998;266:7–12.
[23] Grytsiv A, Kaczorowski D, Leithe-Jasper A, Rogl P, Godart C, Potel M, et al. $EuZn_2Si_2$ and $EuZn_2Ge_2$ grown from Zn or Ga(In)/Zn flux. J Solid State Chem 2002;163:37–43.
[24] Kittel C. Introduction to solid state physics [chapter 9]. New York, Chichester, Brisbane, Toronto, Singapore: John Wiley&Sons, Inc.; 1996. p. 235–279.
[25] White RM. Quantum theory of magnetism [chapter 3]. New York: Springer–Verlag, Berlin, Heidelberg; 1983. p. 67–99.